JTTEES 5:145-153

Characterization of Plasma Sprayed Fe-10Cr-10Mo-(C,B) Amorphous Coatings

K. Kishitake, H. Era, and F. Otsubo

Alloys of Fe-10Cr-10Mo containing a large amount of carbon and/or boron were plasma sprayed by low-pressure plasma spraying (LPPS) and high-energy plasma spraying (HPS). The as-sprayed coatings obtained by the LPPS process are composed of only an amorphous phase, while as-sprayed coatings obtained by the HPS process are a mixture of amorphous and crystalline phases. The amorphous phase in these coatings crystallizes on tempering at about 773 to 873 K, and the crystallization temperatures depend on the content of carbon and boron. Thermal stability of the amorphous phase containing boron is higher than those phases containing carbon.

A very fine mixed structure of ferrite and carbide, borocarbide, or boride is formed by decomposition of the amorphous phase, bringing about a hardness of 1200 to 1400 DPN (Vickers hardness). The coatings containing carbon retain a hardness of more than 1000 DPN, even on tempering at temperatures of 1073 K or higher. The anodic polarization behavior of the coatings exhibits an activation-passivation transition in 1 *N* H_2SO_4 solution. The active and passive current densities of the as-sprayed amorphous and tempered crystalline coatings containing carbon is lower than the coatings containing boron. The corrosion resistance of the as-sprayed and crystallized coatings containing carbon is superior to a SUS316L stainless steel coating.

1. Introduction

IT IS KNOWN that nonequilibrium phases such as amorphous phases (Ref 1, 2), ψ-phase (*A*13 structure, β-Mn type) (Ref 3, 4), χ-phase (*A*12, α-Mn type) (Ref 5, 6), ε-phase (*A*3, hcp) (Ref 7, 8), and γ-phase (*A*1, fcc) (Ref 9, 10) are formed in rapidly solidified high-carbon iron alloys. The authors have investigated the formation and tempering behavior of the nonequilibrium phases in rapidly solidified ribbon of high-carbon iron alloys containing chromium and molybdenum (Ref 11, 12). The nonequilibrium phases showed a high hardness just after decomposition and retained a high hardness up to high temperatures (Ref 2, 4, 12).

The high-carbon iron alloys composed of the nonequilibrium crystalline ε and γ phases were also applied as plasma spray coatings. The coatings retained a high hardness (1100 DPN, or HV) after tempering at temperatures up to 1000 K; just as in the case of rapidly solidified ribbons (Ref 13, 14). The alloy powders have been put into practical use as thermal spray materials for wear resistance at high temperatures (Ref 15). The hardness at high temperatures was attributed to the formation of a large amount of very fine carbides by decomposition of the nonequilibrium phases. Therefore, the amorphous coatings may possess greater hardness properties at high temperatures than the nonequilibrium crystalline coating due to a larger amount of solute elements compared with the nonequilibrium crystalline phases. Also, it is well known that amorphous metal-metalloid alloys have outstanding corrosion resistance. However, there have been no reports on the corrosion resistance of an amorphous metal-metalloid alloy coating prepared by thermal spraying.

On the basis of such experimental results, the present work was carried out to obtain amorphous coatings of iron alloys containing chromium and molybdenum with carbon and/or boron by use of plasma spraying and to investigate its tempering behavior and corrosion resistance.

Keywords amorphous, corrosion resistance, crystallization, iron alloy, plasma spraying

K. Kishitake, H. Era, and **F. Otsubo,** Department of Materials Science and Engineering, Faculty of Engineering, Kyushu Institute of Technology, KitaKyushu 804, Japan.

2. Experimental Procedure

The iron alloy powders were made by a gas atomization method after melting electrolytic iron, graphite, and ferroalloys by using an induction furnace. The chemical compositions of the alloy powders are shown in Table 1.The alloy powders less than 45 μm diameter were used for spraying in this study. The iron alloys have a base composition of 10 wt% Cr and 10 wt% Mo and carbon and/or boron as alloy additions. A small amount of silicon is added to prevent oxidation during powder production. Alloys A, B, and C contain carbon, carbon and boron, and boron,

Table 1 Chemical composition of powders

Alloy	Composition, wt%						Remarks(a)
	Cr	Mo	C	B	Si	Fe	
A	8.37	10.0	4.39	...	0 96	bal	4C
B	10 1	10 0	2 08	1 12	0.73	bal	2C-1B
C	10 1	9 41	..	3 93	0.73	bal	4B

(a) This code refers to the approximate carbon and boron concentrations

respectively. The coatings of about 500 μm thick were obtained on mild steel by using an 80 kW low-pressure plasma spraying (LPPS) and 250 kW high-energy plasma spraying (HPS) under the conditions shown in Table 2. The coatings were heated in vacuum at various temperatures up to 1173 K for 1 h.

The characteristics and structures of the coatings were investigated by means of X-ray diffraction (Fe-kα radiation), microhardness test (30 tests per specimen with a 50 g load) and scanning electron microscopy (SEM). Crystallization behavior of the amorphous phase in the coatings was examined by means of differential thermal analysis (DTA) at a heating rate of 20 K/min. The corrosion resistance of the coatings was evaluated by the anodic polarization curve, which was carried out by use of a potentiostat. Prior to the electrochemical measurement, the coatings were polished with an alumina powder up to 0.05 μm and were masked with an acid-resistant lacquer to form an area of 1 cm^2. The electrolyte used was deaerated 1 N H_2SO_4 solution at 303 K, and the opposite electrode and reference electrode used were platinum and a saturated calomel electrode, respectively. The electrochemical measurement was carried out by scanning the corrosion potential to +1.1 V (versus SCE) with a scanning rate of 60 mV/min after keeping at –0.7 V (versus SCE) for 10 min.

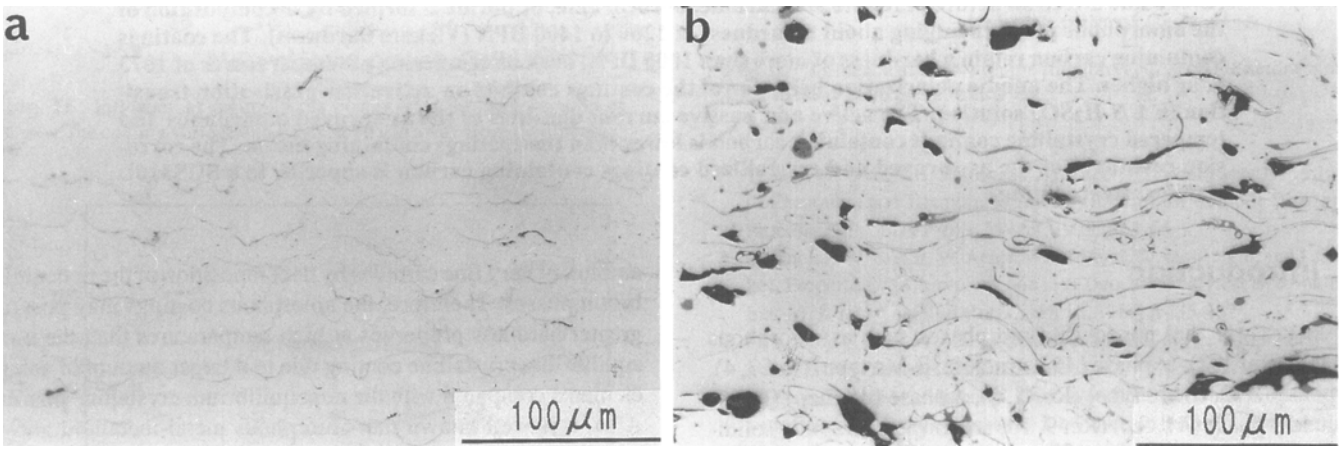

Fig. 1 Optical micrographs of as-sprayed coatings of alloy A. (a) LPPS (b) HPS

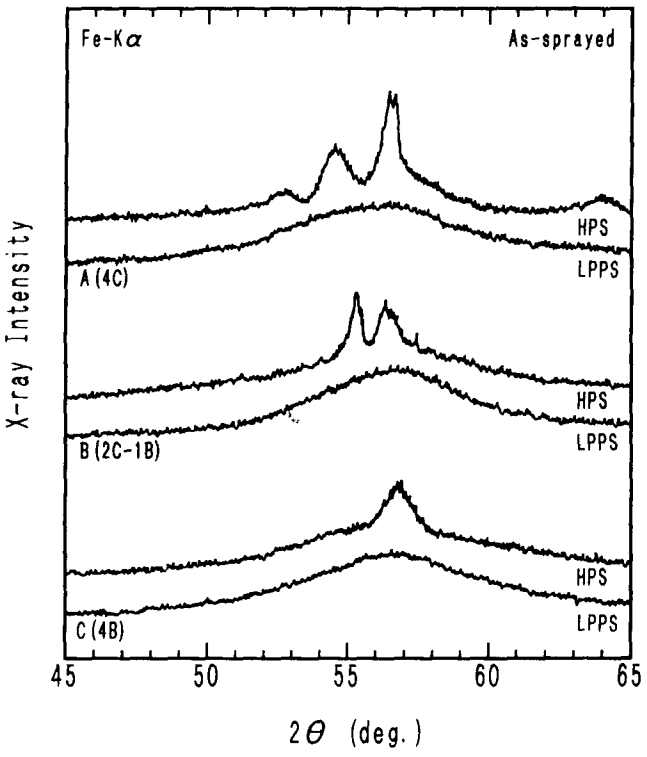

Fig. 2 X-ray diffraction patterns of as-sprayed coatings

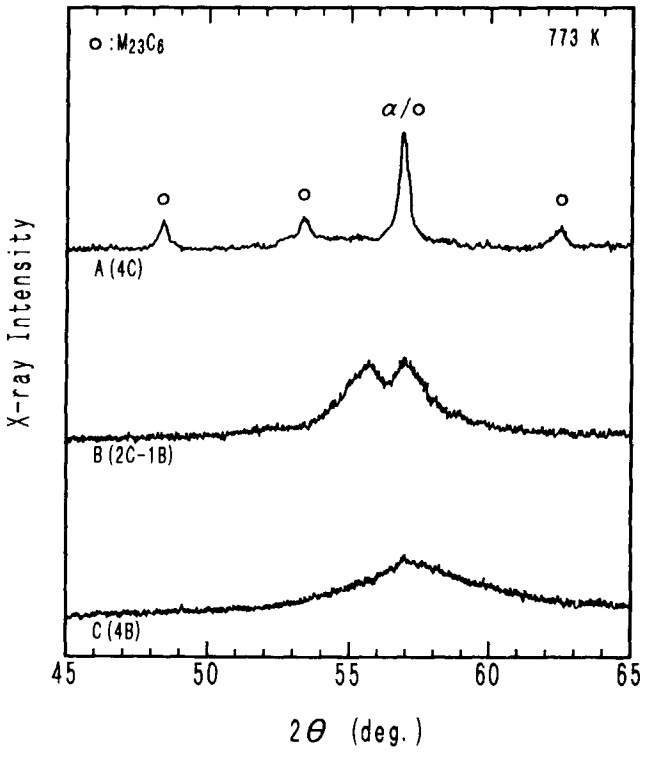

Fig. 3 X-ray diffraction patterns of coatings tempered at 773 K

3. Results and Discussion

3.1 *Structure of the As-Sprayed Coatings*

The structures of the coatings sprayed by LPPS and HPS processes are shown in Fig. 1. Very thin oxide films are visible, but pores are rarely observed in the coatings sprayed by LPPS. On the other hand, some pores and oxide layers exist in the coatings obtained by the HPS process.

The chemical compositions of the as-sprayed coatings are shown in Table 3. The content of chromium, molybdenum, and silicon are virtually unchanged by the plasma spraying process regardless of the LPPS and HPS processes. However, the content of carbon and boron are appreciably reduced by the HPS process.

Figure 2 shows the XRD patterns of the as-sprayed coatings. Only a broad peak, that is, halo pattern, centered on 56 to 57° is observed for the coatings obtained by LPPS. On the other hand, broad diffraction peaks attributed to crystalline phases are observed for the coatings obtained by HPS. It is inferred from the diffraction patterns that perfect amorphous coatings are obtained by the LPPS process and mixtures of amorphous and crystalline phases are formed in coatings obtained by HPS for the three alloys. This difference may result from the difference of the cooling rate between the LPPS and HPS processes and the loss of metalloid elements during HPS.

Table 2 Plasma spraying conditions

LPPS	
Atmosphere	In chamber at 6500 Pa
Currrent, A	1200
Voltage, V	60
Spray distance, mm	300
HPS	
Atmosphere	In the air
Current, A	450
Voltage, V	430
Spray distance, mm	200

3.2 *Decomposition of the Amorphous Phase by Tempering*

X-ray diffraction analysis was carried out to investigate the phases in the amorphous coatings after heat treatment at various temperatures for 1 h. Halo patterns are observed in the diffraction patterns of the amorphous coatings obtained by LPPS even after tempering up to 673 K. On tempering at 773 K, alloy C still retains an amorphous phase and alloy B begins to crystallize, as seen from Fig. 3. However, alloy A crystallizes to form ferrite and $M_{23}C_6$ carbide when tempered at this temperature.

Figure 4 shows the diffraction patterns of the coatings tempered at 873 K. A diffraction peak of M_6C carbide appears in ad-

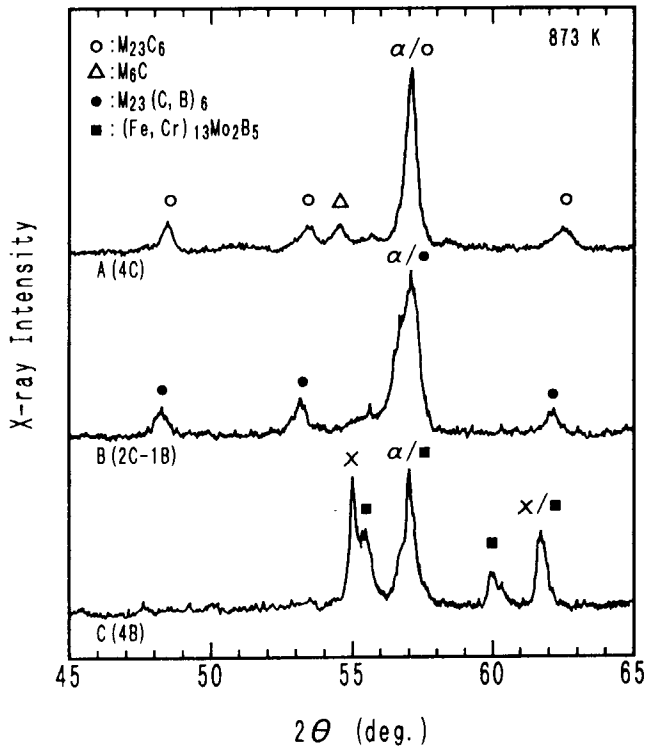

Fig. 4 X-ray diffraction patterns of coatings tempered at 873 K

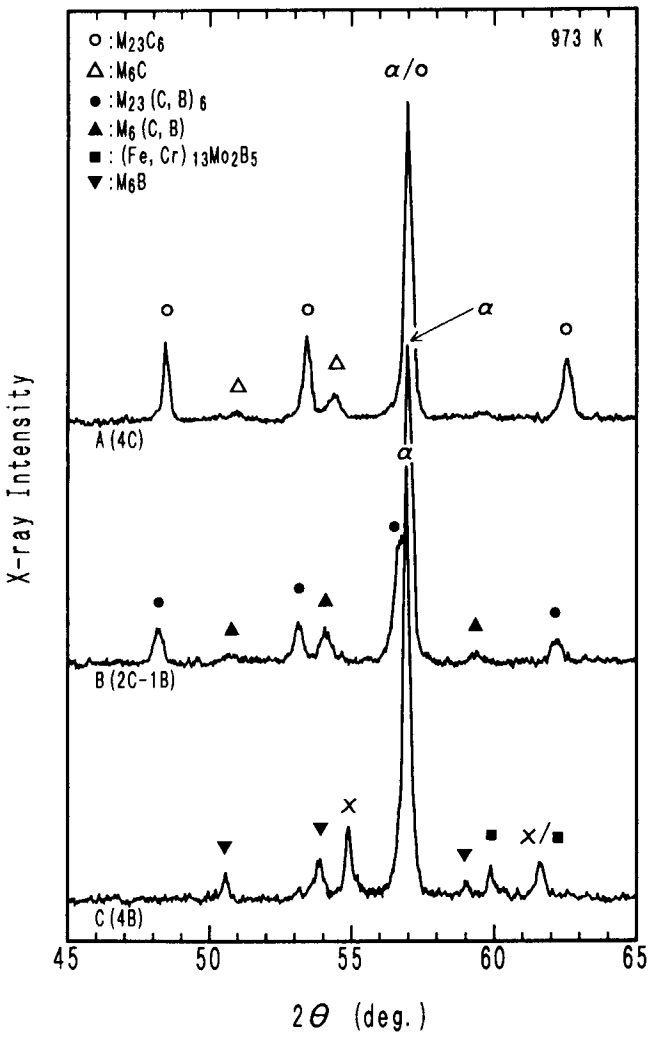

Fig. 5 X-ray diffraction patterns of coatings tempered at 973 K

dition to ferrite and $M_{23}C_6$ in alloy A and the peaks of ferrite and $M_{23}(C,B)_6$ borocarbide appear in alloy B, similarly to the diffraction patterns of alloy A tempered at 773 K. The amorphous phase of alloy C decomposes around this temperature and forms ferrite, α-Mn type χ-phase, and $(Fe,Cr)_{13}Mo_2B_5$ boride.

On tempering at 973 K (Fig. 5), a peak of $M_6(C,B)$ borocarbide appears in addition to ferrite and $M_{23}(C,B)_6$ for alloy B; a similar peak appears for the coating of alloy A tempered at 873 K. It is seen that M_6B phase begins to form with decomposition of χ-phase and $(Fe,Cr)_{13}Mo_2B_5$ phase in the coating of alloy C tempered at 973 K. As shown in Fig. 6, the peaks of ferrite, $M_{23}C_6$ or $M_{23}(C,B)_6$, M_6C or $M_6(C,B)$ become sharp on tempering at 1073 K in alloy A and alloy B. In alloy C, ferrite and M_6B remain after tempering at 1073 K.

On the basis of XRD results, the phases in the coatings are summarized in Table 4. It is clear that on tempering at 773 K, the amorphous phase in the coatings crystallizes in alloy A, begins to crystallize in alloy B, and is still retained in alloy C. Figure 7 shows DTA curves for the coatings. The exothermic peaks of HPS are rather low compared with that of the LPPS peaks because of the small volume fraction of the amorphous phase compared with that of the LPPS material. The beginning temperature of the first exothermic peak, which is attributable to crystallization of the amorphous phase, is seen in the temperature range of about 760 to 820 K for the three coatings. The crystallization temperature of the amorphous phase in the coatings shifts to higher temperature in the order of alloy A, B, C. On tempering at 1073 K, the phases in the coatings are composed of ferrite and carbides, borocarbides, or borides. The volume fraction of carbides, borocarbides, or borides decreases and the volume fraction of ferrite increases in the order of alloy A, B, C, as seen from Fig. 6.

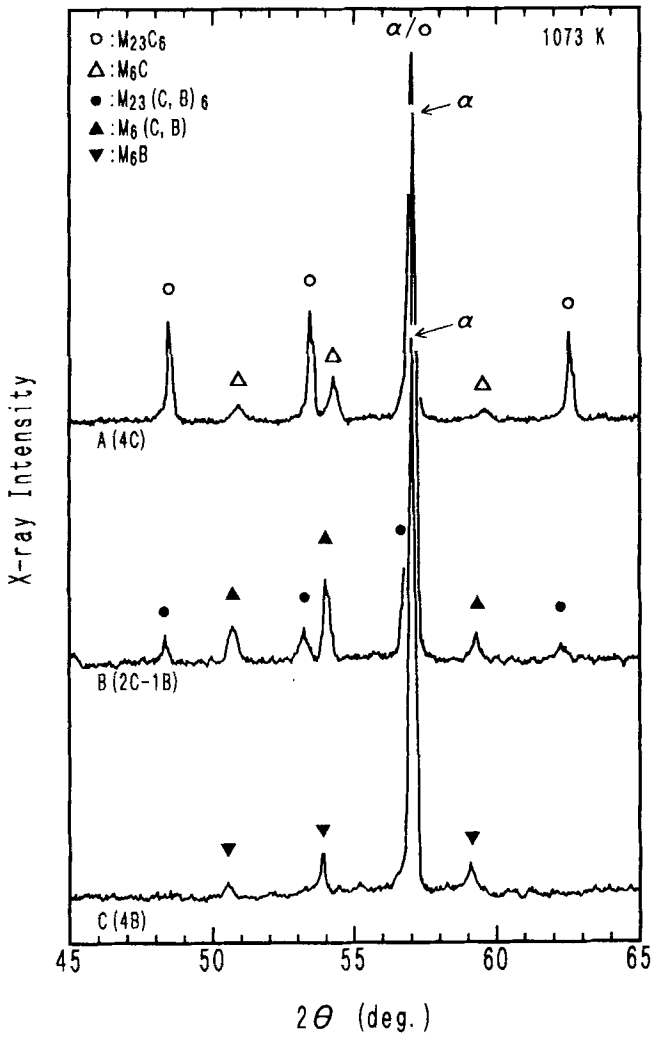

Fig. 6 X-ray diffraction patterns of coatings tempered at 1073 K

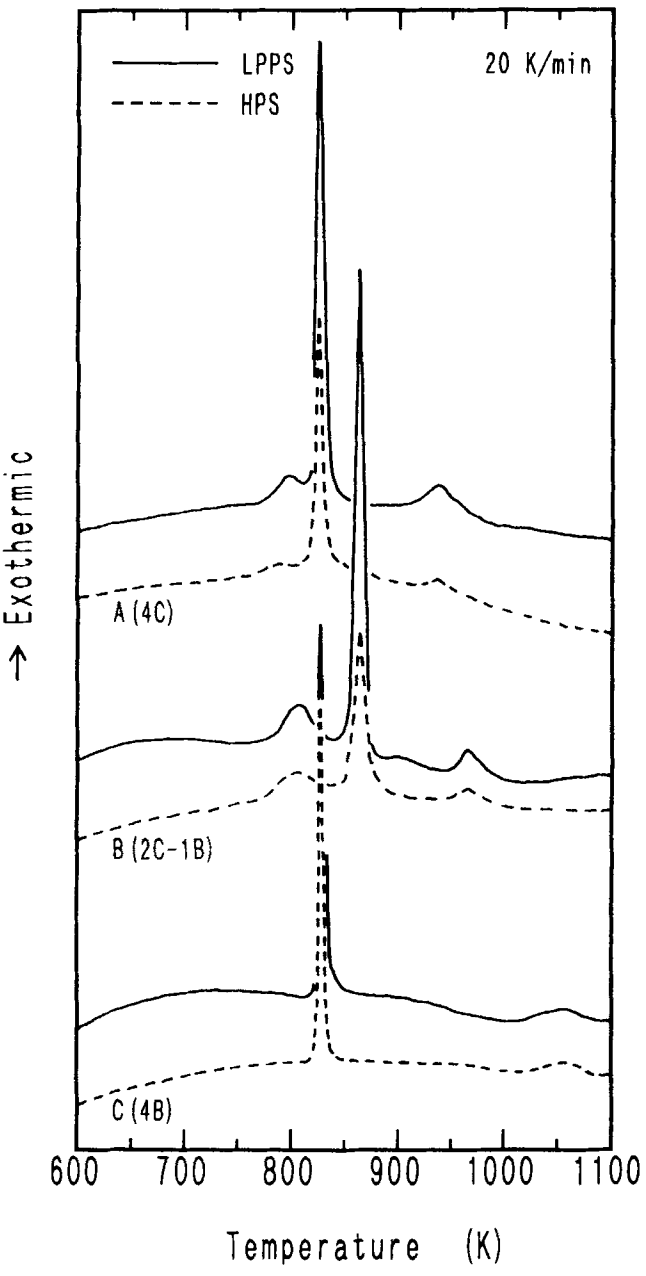

Fig. 7 Differential thermal analysis curves during heating at a rate of 20 K/min

3.3 *Hardness of the Coatings*

Figure 8 shows the effect of tempering on the hardness in the coatings obtained by LPPS. All the as-sprayed coatings revealed a high hardness of around 800 to 900 DPN. The hardness is unchanged by tempering up to 673 K. The hardness of all the coatings begins to increase at 773 K and reaches a peak hardness of about 1400 DPN in alloy A and B on tempering at 873 K. The hardness of alloy C, which exhibited a high crystallization temperature compared with alloy A and B, reaches a peak hardness of about 1300 DPN on tempering at 973 K. It is found that the peak hardness is attained by tempering at a temperature just over the crystallization temperature. The hardness of alloy A and B, however, retains a high hardness of more than 1000 DPN even on tempering at 1173 K. The hardness of alloy C appreciably decreases on tempering at 1073 K or above. Accordingly, it seems that the degradation of hardness predominantly increases with decreasing volume fraction of carbides, borocarbides, or borides. It is important to increase the crystallization temperature of the amorphous phase to achieve a high hardness at a higher temperature, but the addition of boron degrades the hardness on tempering at temperatures of 1073 K.

Figure 9 shows the effect of tempering on the hardness in the coatings obtained by HPS. The hardness of all the coatings is nearly constant up to 673 K and reaches a peak hardness at 873 K to 973 K, and then decreases with tempering temperature; just as in the case of the coatings produced by the LPPS process. The hardness of HPS coatings tempered above the crystallization temperature is lower than that of LPPS coatings. However, even the hardness of the coatings of alloy A processed by HPS revealed a hardness of 1000 DPN or greater after tempering at 1173 K. The difference of the hardness between LPPS and HPS coatings is attributed mainly to the difference of a volume fraction of amorphous phase.

Table 3 Chemical composition of coatings

Alloy	Composition, wt%						Remarks
	Cr	Mo	C	B	Si	Fe	
A(4C)	8 34	10.1	4.34	...	1.02	bal	LPPS
	8.26	10.2	3 51	...	0.92	bal	HPS
B(2C-1B)	9.92	10.6	2 04	0.92	0.78	bal	LPPS
	9.96	10.4	1.96	0.81	0.72	bal	HPS
C(4B)	9.52	10.0	..	3.30	0.78	bal	LPPS
	9.86	9.94	...	2.97	0.74	bal	HPS

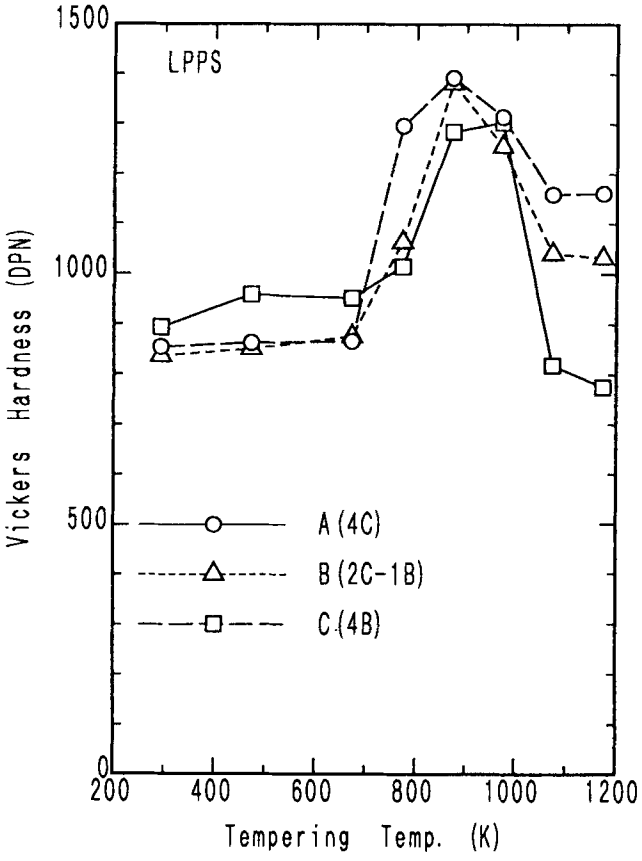

Fig. 8 Change in hardness as a function of tempering temperature (LPPS)

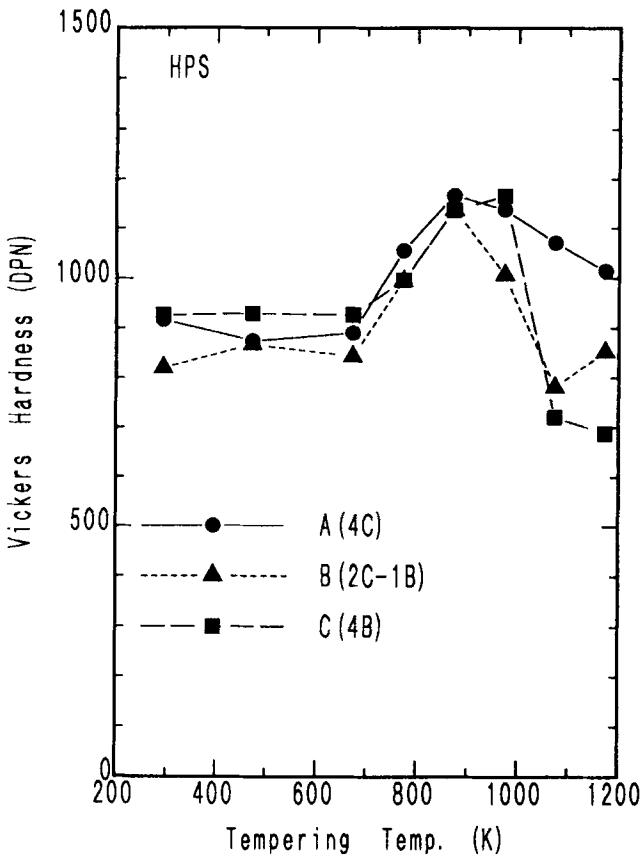

Fig. 9 Change in hardness as a function of tempering temperature (HPS)

Figure 10 shows SEM pictures of LPPS coatings tempered at various temperatures. The coatings, which reached a peak hardness of 1300 to 1400 DPN, reveal a fine structure of ferrite and/or χ-phase and carbides, borocarbides, or borides, as shown in Fig. 10(a), (c), and (e). The enhancement of hardness is attributed to the crystallization of the amorphous phase bringing about a fine structure and a large volume fraction of carbides, borides, or borocarbides. The coatings tempered at 1073 K reveal a coarsened structure compared with those showing the peak hardness, as shown in Fig. 10(b), (d), and (f).

3.4 *Polarization Curves of the Coatings*

Anodic polarization curves of the as-sprayed coatings and subsequently tempered coatings were measured in deaerated 1 N H_2SO_4 solution at 303 K. Figure 11 shows the anodic polarization curves of the as-sprayed coatings obtained by LPPS. An 18-8 austenite stainless steel (JIS-SUS316L) coating is also employed for comparison purposes. The anodic polarization curves of all the coatings exhibit activation-passivation transitions. The coating of alloy A shows the highest corrosion potential and the lowest active and passive current densities. The coating of alloy

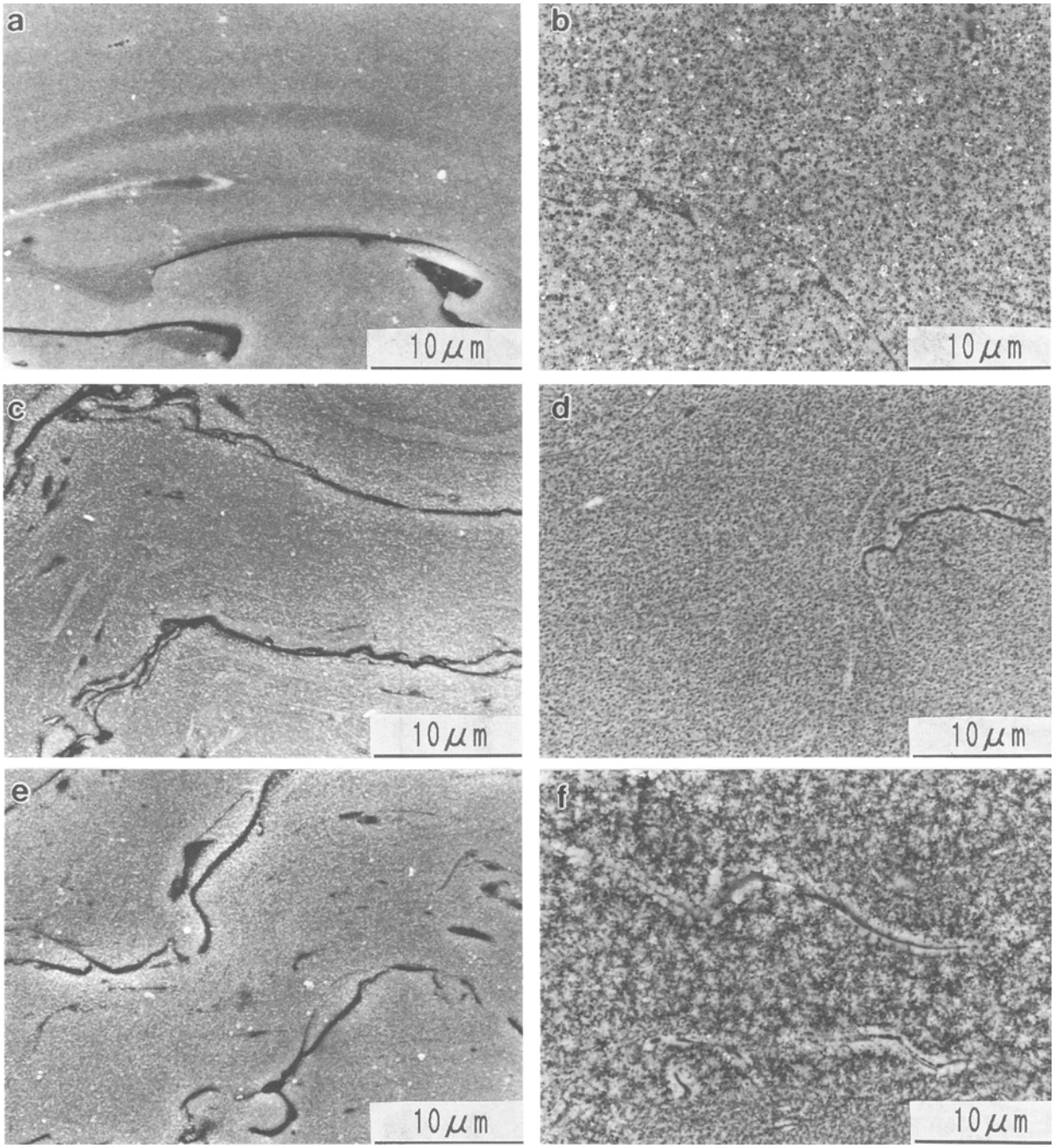

Fig. 10 SEM images of coatings obtained by LPPS at various temperatures (a) and (b) Alloy A (c) and (d) Alloy B (e) and (f) Alloy C. (a), (c), and (e) Peak hardness. (b), (d), and (f) Tempered at 1073 K

C reveals the lowest corrosion potential, and the highest active and passive current densities among these coatings. The anodic polarization curve of alloy B lies between those of alloy A and alloy C. Accordingly, it is found that the addition of carbon is better than boron for corrosion resistance. It is noteworthy that the corrosion resistance of the as-sprayed amorphous coating of alloy A is superior to the SUS316L stainless steel coating.

Figure 12 shows the anodic polarization curves of the as-sprayed coatings obtained by HPS. The three coatings exhibit similar behavior. The active and passive current densities of the HPS coating of alloy A is considerably high compared with the LPPS coating. This deterioration of the corrosion resistance may be due to the existence of crystal phases and oxide as second phases.

Figures 13 through 15 show the effect of tempering on the anodic polarization curves of the LPPS amorphous coatings. The anodic polarization curves of the coatings tempered at 873 and 1073 K reveal two active states, and active and passive current densities of all the crystallized coatings is higher than those of the as-sprayed coatings. The anodic polarization curves of the coatings of alloy B tempered at 873 and 1073 K exhibit appreciably high current density compared with that of the alloy A coatings. The anodic polarization curve of the alloy C coating tempered at 1073 K exhibits higher current density than that of

Table 4 Phases in coatings

Tempering temperature	As-sprayed	Temperature 773 K	873 K	973 K	1073 K	Remarks
A(4C)	Amorphous	α, $M_{23}C_6$	α, $M_{23}C_6$, M_6C	α, $M_{23}C_6$, M_6C	α, $M_{23}C_6$, M_6C	LPPS
	Amorphous, crystalline	α, $M_{23}C_6$	α, $M_{23}C_6$, M_6C	α, $M_{23}C_6$, M_6C	α, $M_{23}C_6$, M_6C	HPS
B(2C-1B)	Amorphous	Amorphous, crystalline	α, $M_{23}(C,B)_6$	α, $M_{23}(C,B)_6$, $M_6(C,B)$	α, $M_{23}(C,B)_6$, $M_6(C,B)$	LPPS
	Amorphous, crystalline	Amorphous, crystalline	α, $M_{23}(C,B)_6$	α, $M_{23}(C,B)_6$, $M_6(C,B)$	α, $M_{23}(C,B)_6$, $M_6(C,B)$	HPS
C(4B)	Amorphous	Amorphous	α, χ, $(Fe,Cr)_{13}Mo_2B_5$	α, χ, $(Fe,Cr)_{13}Mo_2B_5$, M_6B	α, M_6B	LPPS
	Amorphous, crystalline	Amorphous, crystalline	α, χ, $(Fe,Cr)_{13}Mo_2B_5$	α, χ, $(Fe,Cr)_{13}Mo_2B_5$, M_6B	α, M_6B	HPS

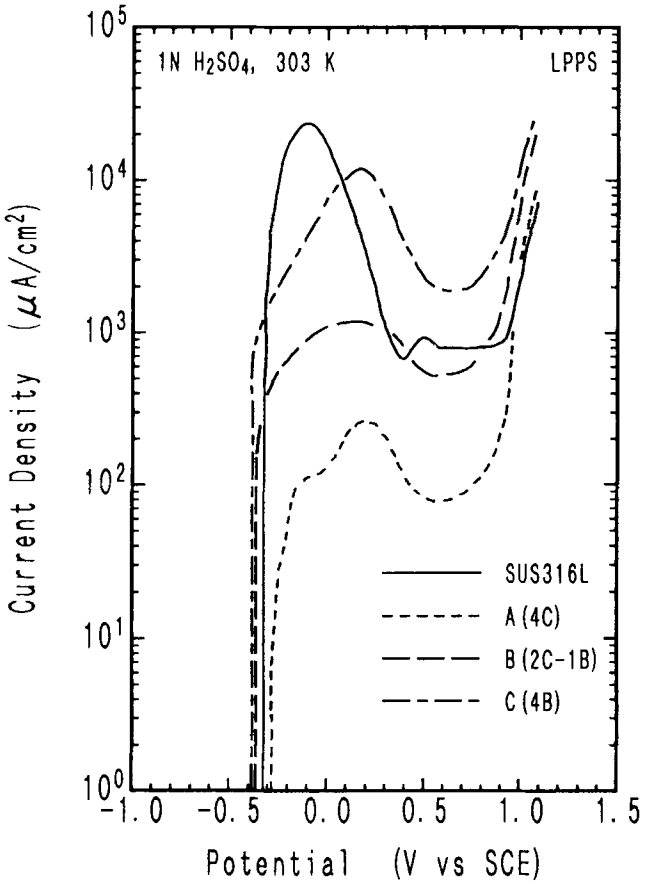

Fig. 11 Anodic polarization curves of as-sprayed coatings (LPPS)

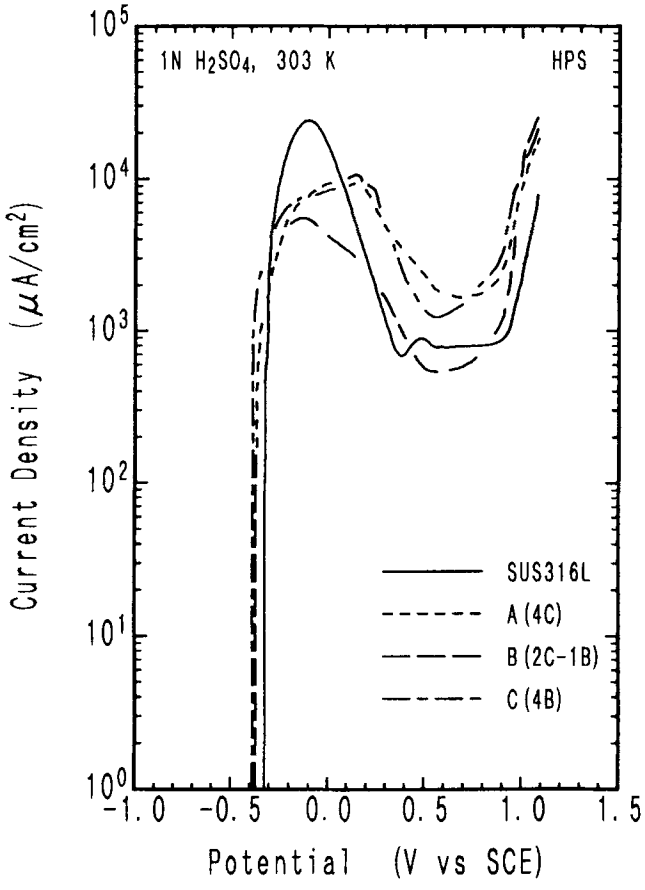

Fig. 12 Anodic polarization curves of as-sprayed coatings (HPS)

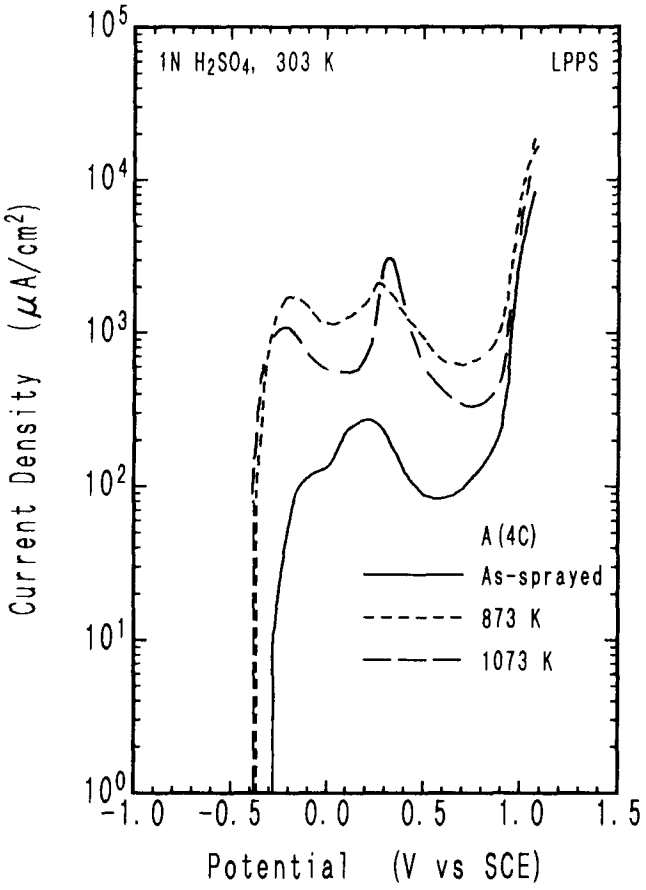

Fig. 13 Anodic polarization curves of coatings of alloy A(4C)

the coating of alloy B. It is found that the corrosion resistance of the LPPS coating of alloy A is the best among the tempered coatings and superior to the SUS316L stainless steel coating. Also, the addition of carbon is more conducive to corrosion resistance in 1 *N* H_2SO_4 solution than the addition of boron, even in tempered coatings having the equilibrium phases.

4. Conclusions

Alloy powders of Fe-10Cr-10Mo containing a large amount of carbon and/or boron were plasma sprayed by LPPS and HPS processes. Tempering behavior and corrosion resistance of the coatings were investigated. The results are summarized as follows:

- An amorphous coating is obtained in the iron alloys by the LPPS process and a mixture of amorphous and crystalline phases is formed in the coatings of the alloys by the HPS process. The as-sprayed amorphous coatings show a high hardness of around 900 DPN.
- The amorphous phase decomposes at 773 to 873 K depending on the composition of the alloys. The LPPS coatings show a high hardness of about 1400 DPN due to a large volume fraction of very fine carbides, borocarbides, or borides resulting from decomposition of the amorphous phase.

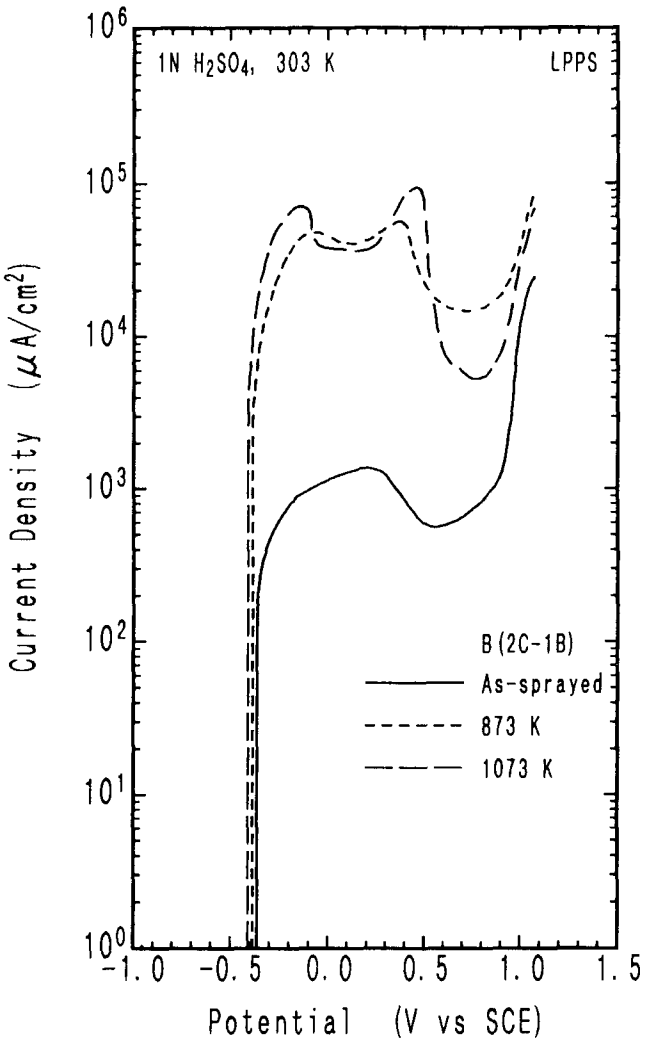

Fig. 14 Anodic polarization curves of coatings of alloy B(2C-1B)

- The addition of carbon allows retention of a higher hardness on tempering at high temperatures of 1073 K or above, compared with boron, because of the smaller volume fraction of ferrite in the coatings with carbon than the coatings with boron.
- The addition of boron deteriorates the corrosion resistance in H_2SO_4 solution of both the as-sprayed amorphous and tempered crystalline coatings compared with carbon. The corrosion resistance of as-sprayed amorphous and tempered crystalline coatings of alloy A(4C) is superior to a SUS316L stainless steel coating in H_2SO_4 solution.

Acknowledgments

This work was supported by the Grant-in-Aid of the Ministry of Education in Japan. The authors wish to acknowledge the Plant and Machinery Division of the Nippon Steel Corporation for preparing samples and Mr. K. Nakashima and Mr. T. Kichise, formerly students of Kyushu Institute of Technology, for experimental assistance.

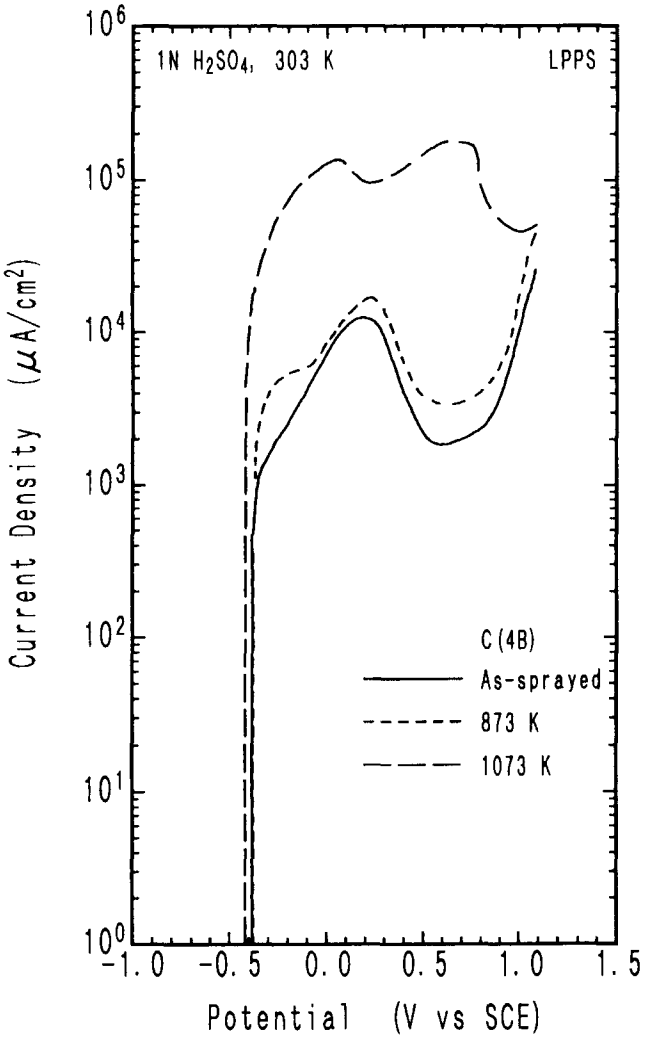

Fig. 15 Anodic polarization curves of coatings of alloy C(4B)

References

1 A. Inoue and T. Masumoto, Crystallization Behavior of Amorphous High-Carbon Alloy Steels, *Sci. Rep. Res. Inst. Tohoku Univ.*, Vol A27, 1979, p 147-158

2 K Kishitake, H. Era, and F Otsubo, Enhancement of Hardness by Heat Treatment in Rapidly Solidified High-Carbon Iron Alloys, *Scr. Metall. Mater.*, Vol 24, 1990, p 1269-1273

3 H Era, K Kishitake, F. Otsubo, and E Tanaka, A13-Type Phase Revealed in Rapidly Solidified High-Carbon Iron Alloy, *Metall. Trans. A*, Vol 22A, 1991, p 251-253

4 H Era, K Kishitake, and P. Li, Structure and Decomposition of A13-Type Phase in Rapidly Solidified High-Carbon Cr-Si Iron Alloy, *Metall. Trans. A*, Vol 24A, 1993, p 751-756

5. T. Iwadachi, A Inoue, T. Minemura, and T Masumoto, Nonequilibrium Phases in Fe-X-C (X = Cr, Mo,W) Ternary Alloys Quenched Rapidly from Melts, *J. Jpn. Inst. Met.*, Vol 44, 1980, p 245-254 (in Japanese)

6 A. Inoue, L. Arnberg, M Oguchi, U. Backmark, N. Bäckström, and T Masumoto, Preparation of Fe-Cr-Mo-C Amorphous Powders and Microstructure and Mechanical Properties of their Hot-Pressed Products, *Mater. Sci. Eng.*, Vol 95, 1987, p 101-114

7 R.C. Ruhl and M Cohen, Splat Quenching of Iron-Carbon Alloys, *Trans. Metall. Soc. AIME*, Vol 245, 1969, p 241-251

8. K Kishitake, H Era, F Otsubo, and E Tanaka, Nonequilibrium Austenite/ε-Phase Eutectic Revealed in Rapidly Solidified High-Carbon Iron Alloy, *Metall. Trans. A*, Vol 22A, 1991, p 791-792

9. T. Minemura, A. Inoue, and T. Masumoto, Metastable Austenite Phase in Rapidly Quenched Fe-Cr-C Alloys, *Trans. ISIJ*, Vol 21, 1981, p 649-655

10 T. Minemura, A. Inoue, Y. Kojima, and T. Masumoto, Microstructure and Mechanical Properties of Nonequilibrium Austenite in Fe-C-(Mo.W) Systems Rapidly Quenched from Melts, *Trans. ISIJ*, Vol 22, 1982, p 934-941

11. K. Kishitake, H Era, and P Li, Nonequilibrium Phases in Rapidly Solidified High-Carbon Fe-Cr-Mo Alloys, Materials, *Trans. JIM*, Vol 34, 1993, p 54-61

12 K Kishitake, H Era, and F. Otsubo, Structures and Tempering Behavior of Rapidly Solidified High-Carbon Iron Alloys, *Metall. Trans. A*, Vol 22A, 1991, p 775-782

13 H Matsumoto, K. Kishitake, T. Irisawa, and H. Era, Characteristics of Rapidly Solidified Coatings Obtained by Thermal Spraying of White Cast Irons, *J. Jpn. Foundry. Soc.*, Vol 62, 1990, p 37-42 (in Japanese)

14 K. Kishitake, H. Matsumoto, H. Era, and T. Irisawa, Characteristics of Rapidly Solidified Coatings Obtained by Thermal Spraying of White Cast Irons Containing Carbide Former Elements, *J. Jpn. Foundry. Soc.*, Vol 62, 1990, p 185-190 (in Japanese)

15. H. Matsumoto and K. Kishitake, "Thermal Sprayed Coating of High-Carbon Iron Alloy," Japanese patent 6-65747, 1994 (in Japanese)